Efficiency analysis and optimisation of DEM for railway ballast track simulations
Multi-layer shape model of lateral resistance

Jia, Wenli; Markine, Valeri; Guo, Yunlong

DOI
10.1016/j.trgeo.2023.100977

Publication date
2023

Document Version
Final published version

Published in
Transportation Geotechnics

Transportation Geotechnics 40 (2023) 100977

Contents lists available at ScienceDirect

Transportation Geotechnics

journal homepage: www.elsevier.com/locate/trgeo

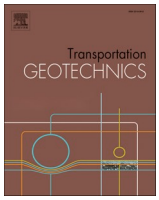

Efficiency analysis and optimisation of DEM for railway ballast track simulations: Multi-layer shape model of lateral resistance

Wenli Jia [a,*], Valeri Markine [a], Yunlong Guo [a,*]

[a] Faculty of Civil Engineering and Geosciences, Delft University of Technology, Delft 2628CN, Netherlands

ARTICLE INFO

Keywords:
Railway ballast
DEM
Simulation efficiency
Model optimisation
Railway track

ABSTRACT

The railway ballast layer provides the function of bearing loading, resisting geometry degradation, and drainage. In those related research, the behaviour of ballast assembly can be obtained by laboratory (or in-situ) tests. Limited simulation methods can be used to analyse the behaviour of ballast particles at the mesoscopic level. The numerical simulations based on the Discrete Element Method (DEM) are employed, which treat every ballast particle as a calculation component. However, the efficiency of DEM simulation is very low due to the algorithm and a very large number of elements. This paper analysed the efficiency-related questions of the DEM modelling. The influence of particle shape and contact properties on the force behaviour is studied. Further, an optimised multi-layer ballast track model is introduced based on the most influential ballast areas. In such areas, particles are generated with an irregular shape to ensure the reliability of results, and particles except that area are generated with a rolling resisted ball shape to decrease the number of elements. A series of lateral resistance simulations are conducted to show and validate the accuracy and efficiency of this method in the dimension of the single sleeper section. Results show that this optimised multi-layer model building method largely improves efficiency, and it can provide accurate data.

Introduction

Railway ballast, produced by crushed hard stones, is the building material of the substructure of railway tracks. The ballast layer is the compacted assembly of ballast particles, which performs the function of bearing and elasticity to rail, redistributing the force transmitted from the sleeper, providing resistance to the sleeper to keep the track geometry, and providing drainage ability and maintenance ability [1]. In order to fulfil those functions, ballast particles should have properties of enough strength, a coarse surface, and an angular shape. In addition, the assembly should be within a range of Particle Size Distribution (PSD) [2].Fig. 1.

The research methods for railway studies typically include tests (laboratory and in-situ) and numerical simulations (Discrete Element Method and Finite Element Method) [3–7]. Especially for railway ballast, research is commonly conducted with DEM simulations. Because in the DEM model, the ballast layer is built by particles, thus the contact behaviour between particles can be found. This mesoscopic numerical tool makes up for the limitation of tests and FEM.

In order to capture accurate results, the DEM model should present the irregular shape of the ballast, and a proper contact model should be applied to simulate the physical reality. For example, in reference [8], as shown in Fig. 2, the scale of the model is a single sleeper section, the ballast particles are generated based on templates from real ballast 3D scanning, and the linear contact model is verified by in-situ tests. That model can be regarded as a high-fidelity model, where the spatial and transient information is simulated accurately.

However, due to the complexity of the particle shape of the high-fidelity model and the algorithm of DEM, the efficiency of DEM simulations has become a major problem. The DEM simulations of a large-scale model (or the long-term behaviour) show an unacceptable time cost (maybe years). Under this limitation, the DEM model for ballast research is normally built on a small scale, such as the direct shear test, triaxial compression test, ballast box text, etc.

The model simplification methods are studied on how to use a low-fidelity model to present the aiming results [9–11]. The low-fidelity model can increase efficiency by missing some physical performance. For example, up-scaling the particle size can decrease the particle number, thus decreasing the calculation cost. However, the low fidelity model may not present the physical reality, but methods can be built

* Corresponding authors.
E-mail addresses: j.jia-1@tudelft.nl (W. Jia), Yunlong.Guo@tudelft.nl (Y. Guo).

https://doi.org/10.1016/j.trgeo.2023.100977
Received 1 February 2023; Received in revised form 24 February 2023; Accepted 5 March 2023
Available online 10 March 2023

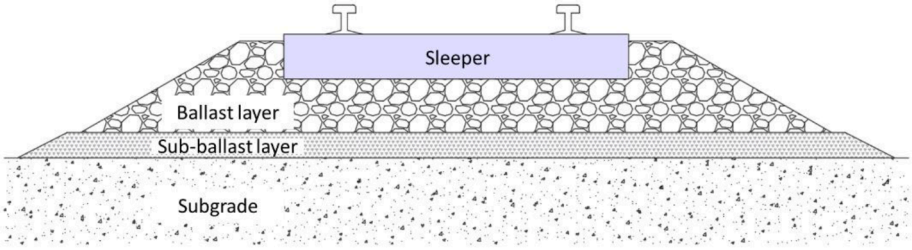

Fig. 1. Ballast track.

Fig. 2. DEM model of a single sleeper(wing-shape) section [8].

biased to the target by modelling approaches. It contains 2 main types:

First is the model fitting. This method uses a mathematical relation to calculate the relationship between results obtained from the simplified model and the accurate model (or experimental tests). Thus, proper parameters are needed, and the results typically are key performance indicators. The description of this method is shown in the following Eq. (1).

$$F(x) \sim \widetilde{F}(x,a) = \widetilde{F}(f(x),a) \tag{1}$$

The second method is the reduce order modelling. This method is based on the simplified model (such as, in state space dimension, degrees of freedom), while it still includes the needed spatial and transient information. The description of this method is shown in the following Eq. (2).

$$F(x) \sim \widetilde{F}(x,a) = \widetilde{F}(f(x),a) + C(x,a) \tag{2}$$

Based on those simplification methods, particle size is the first choice to be focused on, which can solve the efficiency problem for powder and soil materials simulations. Reference [12] uses the up-scaling method to reduce the number of elements in a model of large-scale bulk handling equipment and the iron ore pellets model. When using the up-scaling method, the efficiency increased by 55 times (77 m^3 powders and grab tool). In reference [13], the soil particle uniformly ranges from 10 mm to 20 mm. The fine particles are discarded to increase efficiency and are regarded as not critical to aiming results. In addition, the cohesion behaviour between particles is simulated by adding a parallel bond parameter to the contact model. In reference [14], the influence of soil particle size on soil-subsoiler interactions is analysed, and the results indicated the most proper particle size and its efficiency.

Focusing on ballast-related research, the simplification method based on particle size is not a proper choice because the PSD is a key factor, and several characteristics of the ballast layer are size-related. In addition, the size ratio between ballast and sleeper (or other test devices) is relatively small compared with the size ratio between soil (or powder) and related tools. In Reference [15–18], the shear boxes are 5 to 10 times bigger than the largest ballast particle size. In comparison, to obtain an accurate result of sand (or soil), the shear box has to be at least 40–60 times bigger than the largest particle size [19].

Under the above considerations, the simplification method for ballast is normally in 2 types. The first method is using a 2D model instead of a 3D model. In reference [20], a 2D DEM model is used to analyse the breakage behaviour under cyclic loading. In reference [21], a 2D DEM model is used to simulate the direct shear tests and cyclic loading for settlement tests. This dimensional simplification can highly improve the efficiency, making the simulation of long-term behaviour possible, but the problem of accuracy of the 2D model is obvious due to 1-dimension loss.

The second method is reducing the complexity of the irregular shape, using a ball or a simple group of balls to represent the irregular real ballast shape, such as in reference [22], a 2-ball generated particle is used to present the ballast shape. Also, in the reference, a cross-section of 0.15 m in width of the ballast track is used to increase efficiency. In reference [23], a cluster of disks is used to present the ballast shape. The number of disks of a cluster ranges from 2 to 9 according to the particle size. Also, in the reference, the simulations are carried out in 2D to increase efficiency.

In addition, the model calibration methods are typically taken into consideration because the ballast properties are influenced by the simplified shape. Such as, the repose angle is used to qualify the behaviour in reference [24–26]. However, there is also evidence that the macroscopic results of an assembly can be obtained and verified, but the contact between the particle is inconsistent with mesoscopic results [27]. The shape simplification method improves efficiency by reducing the number of elements, but the shape loss will lead to unclear force behaviour (as illustrated in chapter 2).

Overall, the DEM modelling method limitation is due to the low efficiency, and previous simplification methods to improve the efficiency have drawbacks. Based on the above-mentioned background, the aiming of this paper is to improve the efficiency of DEM calculations. Firstly, this paper analyses the influence of particle shape on force behaviour by using a ballast box model, and the particle shape is selected. In addition, the contact model and its parameters are introduced. Based on the particle shape, the linear contact model for the irregular shape and the linear contact model with rolling resistance for the ball shape are analysed based on the literature review. Finally, a multi-layer model of a single sleeper section is built, and the efficiency and reliability are validated.

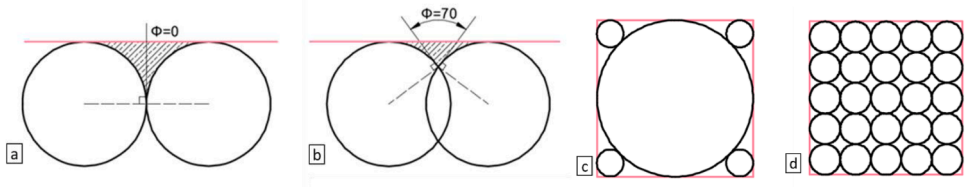

Fig. 3. Definition of the distance and ratio: a) Distance = 0, b) Distance = 70, c) Ratio = 0.2, d) Ratio = 1 [18].

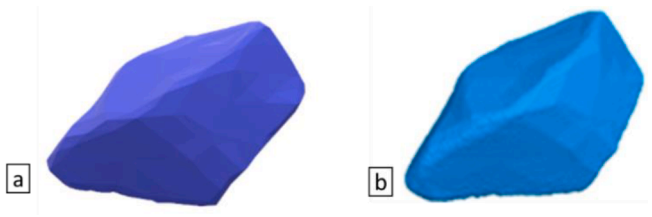

Fig. 4. A real shape clump generated in PFC3D software, (a) Geometry from 3D scanning, (b) Clump with 13,148 balls.

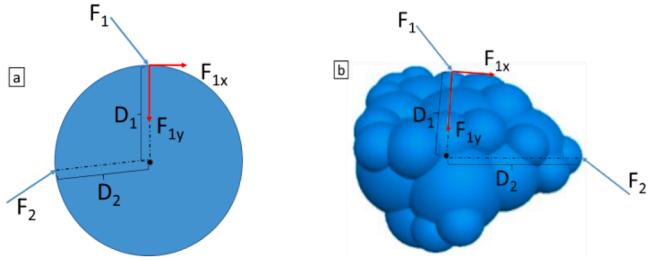

Fig. 5. Applied force on the sphere and irregular shape: a) ball shape, b) clump shape.

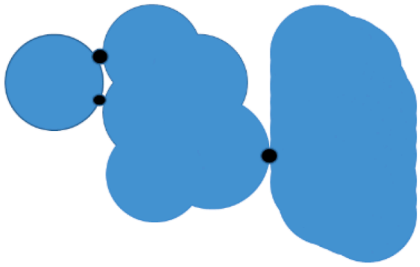

Fig. 6. Different contact caused by spherical surface (black dot: contact point).

Particle shape

Particle shape is the key factor related to the accuracy of the results because the irregular ballast particle shape provides the uneven force transmission and force re-distribution path. And the interlock caused by angular limits the displacement and rotation of ballast, thus providing strength and elasticity.

The basic DEM particle is a ball, and a cluster of balls can be generated as the clump element by controlling the arrangement of balls in a template. In the arrangement rules, the distance parameter controls the overlap, and the ratio parameter controls the radius, as illustrated in Fig. 3 [18]. By this method, a clump particle can be generated very close to a real ballast shape, with considerable balls, as shown in Fig. 4.

The high-fidelity particle contributes to high accuracy. Firstly, the irregular shape contributes to force transmission. The comparison between a ball shape and an irregular shape illustrates it. As shown in Fig. 5, once the relative position between the 2 components and the centre of mass is the same, the motion and force transmission will be relatively the same. Wherever the force is applied, this relative position has a high possibility of being the same in a ball but a very low possibility of being the same in an irregular shape.

Secondly, the angular shape is related to the contact force distribution between particle–particle because a curved surface will lead to more contact points. As shown in Fig. 6 (the black dots are the contact point), if the particle surface consists of serval spherical surfaces, the contact points will change (also shown in Table 1: total contact number) and lead to different behaviours of compressional and frictional force.

A comparison between different degrees of simplifications is used to illustrate the difference. In this series of simulations, the 3 models were built all the same, except for the particle shape. It shows the contact behaviour when a wedged shape sleeper inserts into the ballast layer. The contact parameters are listed in following Table 2 (Chapter 3). This box model contains 3 parts, the sleeper, ballast box, and ballast particles, as shown in following Fig. 7, and the Particle Size Distribution(PSD) is shown in Fig. 8 (all the models in this paper use the same PSD). After the model reaches an initial balanced state, a 4 mm/s velocity is applied to the sleeper. Firstly, the sleeper is lifted 4 mm, then lowered to compact

Table 2
Contact parameters.

Parameters	Ballast (Clump)	Ballast (ball)	Sleeper
Tangential stiffness(N/m)	2e7	2e7	5e9
Normal stiffness(N/m)	2e7	2e7	5e9
Friction coefficient (Linear contact)	0.5	0.5	0.5
Friction coefficient (Rolling resistance)	–	0.3	–
Mass density(kg/m^3)	2800	2800	NA
Weight (kg)	–	–	380
Damping coefficient	0.7	0.7	–

Table 1
Influence of different particle shapes on contact behaviour.

Shape description	Ball	Clump (spherical surfaces)	Clump (non-spherical surfaces)
Representative particle shape			
D/R value	NA	D120/R0.5	D130/R0.4
Contact force distribution	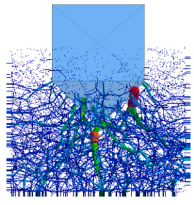	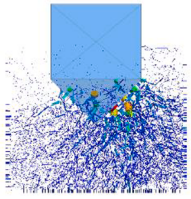	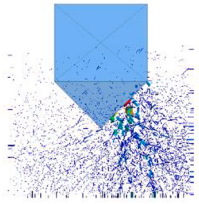
Total contact number	5991	11,573	10,536
Maximum contact force particle–particle (kN)	1.3	13.0	21.9
Maximum contact force particle-sleeper (kN)	13.5	101.6	80.1

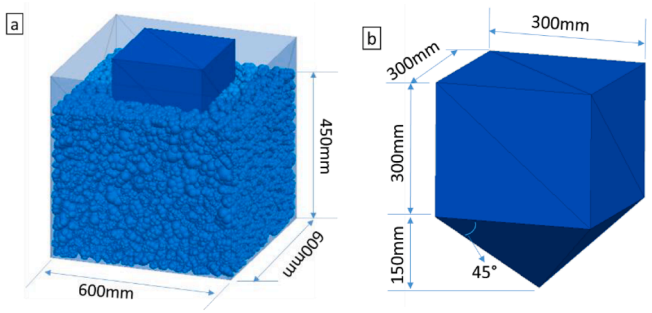

Fig. 7. Ballast box model: a) sleeper, b) Ballast box.

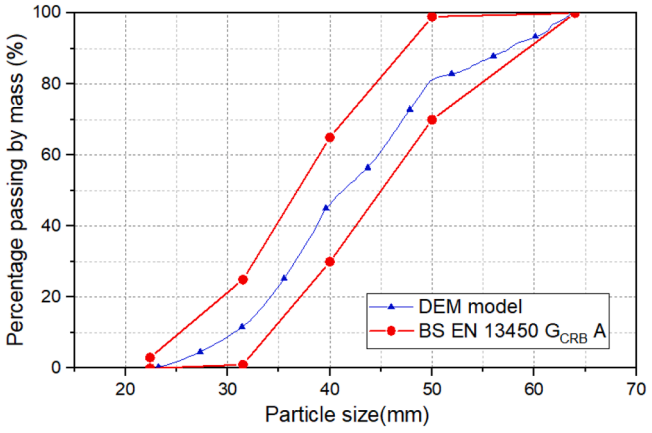

Fig. 8. Particle size distribution (PSD).

the ballast, and finally, stop the sleeper when it reaches the initial location. This process simulates the sleeper-ballast contact behaviour under 4 mm settlement. The ending state of the model was saved to show the influence of particle shape on contact behaviour.

Under the same sleeper displacement, the results are concluded in Table 1. The Distance/Ratio and 3 representative particles are listed. By using those different simplifications of particle shapes, results show differences in several aspects, such as the force distribution, maximum contact force, and displacement.

As shown in Table 1, the number of contacts in the ball-built model is 5991, whereas the value of the clump-built model with spherical surfaces is 11573, and the value of that with non-spherical surfaces is 10536. The contact number of the ball-built model is 48% and 43% less than the clump-built model. Also, the clump with a spherical surface provides more contact points than that of a clump with non-spherical surfaces, but the force distribution changes from uniform to chain form. This unclear force distribution disobeys the physical behaviour of a ballast assembly. It should be avoided in ballast research.

The shape influences the force behaviour because of the contact number and force distribution difference. The maximum contact force between the particle–particle of the ball-built model is 1.3kN, compared with the value (13.0 kN and 21.9kN) of the clump-built model, which decreases between 90% and 96%. Similar results also can be observed in the maximum contact force between the particle-sleeper, the value of the ball-built model is 13.5kN, and the clump-built model is 101.6kN and 80.1kN. Those results show the influence of particle shape. It also contributes to the importance of using irregular ballast particle shapes.

However, complex particle shape leads to a higher number of elements in a DEM model, and the higher number leads to higher calculation costs. The efficiency and simplification of ballast particle shape are developed in the following chapter. It combines the high-fidelity part and low-fidelity part in a model, realised by using the irregular shape in the most influential area and the ball particle in other less influential areas.

Contact properties

The complexity of particle shape influences the total number of elements in a model, thus influencing the calculation efficiency. The contact parameters are also vital to efficiency. Because the force and displacement behaviours should be calculated and updated based on a defined timestep, if the timestep is too long, the high increment of force and displacement leads to the model explosion.

Considering that the ballast layer is a non-cohesive granular assembly, the linear contact model can be used to simulate the contact behaviour between ballast particles (or ballast-sleeper). Those contact parameters contain the shear stiffness, the normal stiffness, the friction coefficient, and the reference gap. Contact parameters work together with the physical parameters of elements, which include density and particle size distribution. Under external conditions, for example, the applied force, the sample will show its performance. The details of the calculation are as follows.

In the linear contact model, the contact force is calculated based on: F^l is the linear force. As the following Eqs. (3) and (4).

$$F^l = -F_n^l \hat{n}_c + F_s^l,\ M_c \equiv 0 \tag{3}$$

$$F_s^l = -F_{ss}^l \hat{s}_c + F_{ss}^l \hat{t}_c \tag{4}$$

Where: F_n^l is the normal component, when $F_n^l > 0$ is tension.

F_s^l is the shear component.

The displacement of a particle is a universal value. Within a timestep Δt, the displacement is calculated with the relative increase value $\Delta\delta$, and the surface gap g_s, which is set to define whether a contact is valid. As the flowing Eqs. (5) and (6):

$$\Delta\delta_n = \alpha\Delta\delta_n;\ \Delta\delta_s = \alpha\Delta\delta_s \tag{5}$$

$$\alpha = \begin{cases} \dfrac{g_s}{g_s - (g_s)_o}, & (g_s)_o > 0 and g_s < 0 \\ 1, otherwise \end{cases} \tag{6}$$

Where, $(g_s)_o$ is the surface gap at the beginning of one timestep.

The force–displacement law of the linear model consists of the following steps:

Update the linear normal force based on the normal-force update mode. As the flowing Eq. (7).

$$F_n^l = \begin{cases} \begin{cases} k_n g_s, g_s < 0 \\ 0, otherwise \end{cases}, M_l = 0 (absolute\ update) \\ \min\left(\left(F_n^l\right)_o + k_n\Delta\delta_n, 0\right), M_l = 1 (increase\ update) \end{cases} \tag{7}$$

Where, k_n is the normal stiffness,

$(F_n^l)_0$ is the linear normal linear contact force at the beginning of the timestep.

Update the linear shear force. As the flowing Eqs. (8)–(11).

$$F_s^* = \left(F_s^l\right)_o - k_s\Delta\delta_s \tag{8}$$

$$F_s^\mu = -\mu F_n^l \tag{9}$$

$$F_s^l = \begin{cases} F_s^*, \left\|F_s^*\right\| \le F_s^\mu \\ F_s^\mu \dfrac{F_s^*}{\left\|F_s^*\right\|}, otherwise \end{cases} \tag{10}$$

$$s = \begin{cases} true, \left\|F_s^l\right\| \le F_s^\mu \\ false, otherwise \end{cases} \tag{11}$$

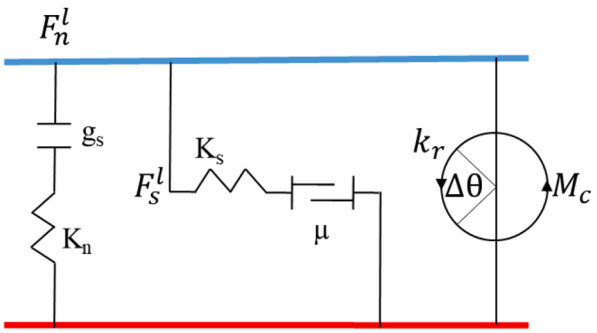

Fig. 9. Linear contact with rolling resistance.

Where, s is the state of slip determination,

μ is the friction coefficient,

k_s is the shear stiffness,

Based on that, to keep the model stable, the timestep in a calculation cycle will be influenced by contact parameters and kinematic behaviour, and the kinematic-related timestep is calculated as the following Eqs. (12)–(14):

$$a_i = \frac{\left(F_i + g_i m_g + F a_i\right)}{m_i} \tag{12}$$

$$t = \frac{\left(-v_0 + \sqrt{v_0^2 + 2a_0 x)} \right)}{a} \tag{13}$$

$$t_{kin} = \frac{\left(-v_{max} + \sqrt{v_{max}^2 + 2a_{max}\varepsilon)} \right)}{a} \tag{14}$$

Then, the actual timestep used in any cycle is taken as a fraction of this estimated critical value, which is the stiffness constraint, as the following Eq. (15), in 1-dimension.

$$t_{crit} = \min\left(\sqrt{\frac{m}{k}}\right)(1 - dimensional) \tag{15}$$

With this method, the stiffness will be estimated by summing the contribution from all contacts using only the diagonal terms of the contact stiffness matrix. The final critical timestep is taken to be the minimum of all critical time steps computed for all degrees of freedom of all bodies.

The stiffness used for ballast particles is set with a certain value. For example, in reference [28], the normal stiffness and shear stiffness are 2e6 and 1e6 for ballast-ballast contacts. In reference [29], the research defined the normal stiffness 4.2e7 as and shear stiffness are 5.5e7. On the other hand, reference [30] summarised the contact stiffness value that the commonly used stiffness ranges from 1e6 to 5e9. Within the

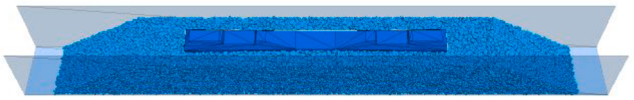

Fig. 11. Clump-built model of a single sleeper section.

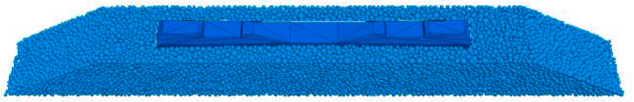

Fig. 12. Ball-built model of a single sleeper section.

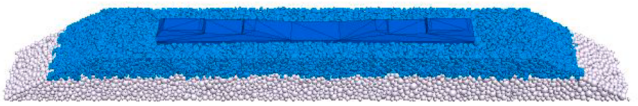

Fig. 13. Multi-layer model with clumps and balls of a single sleeper section model.

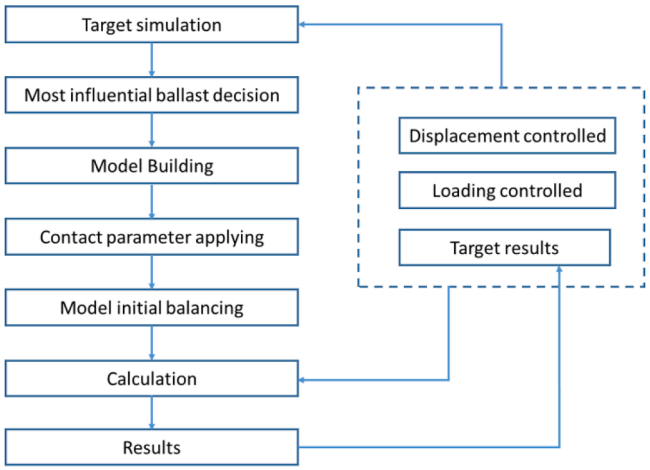

Fig. 14. Process of multi-layer model simulation.

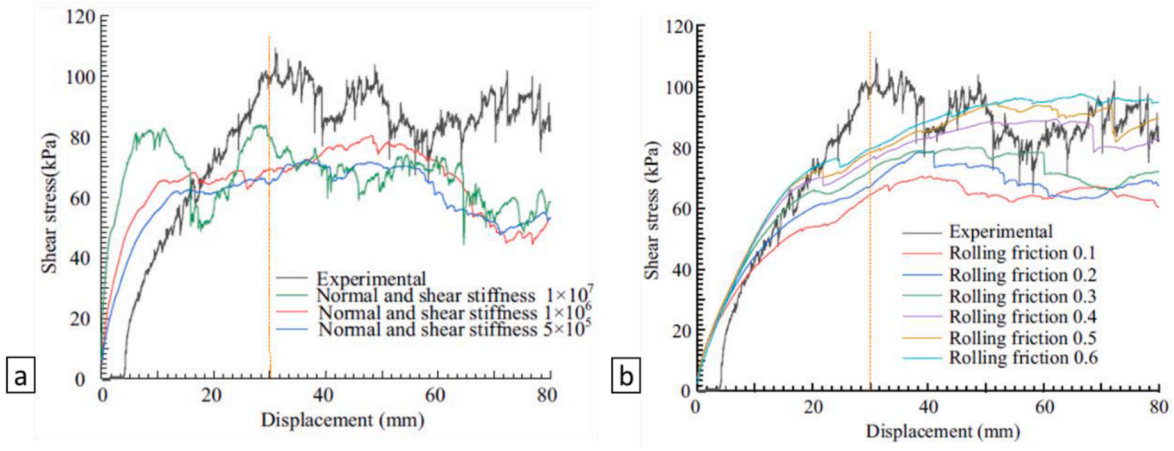

Fig. 10. Shear stress influenced by: a) Stiffness, b) Rolling friction coefficient [32].

Fig. 15. PIV setting on lateral resistance test [34].

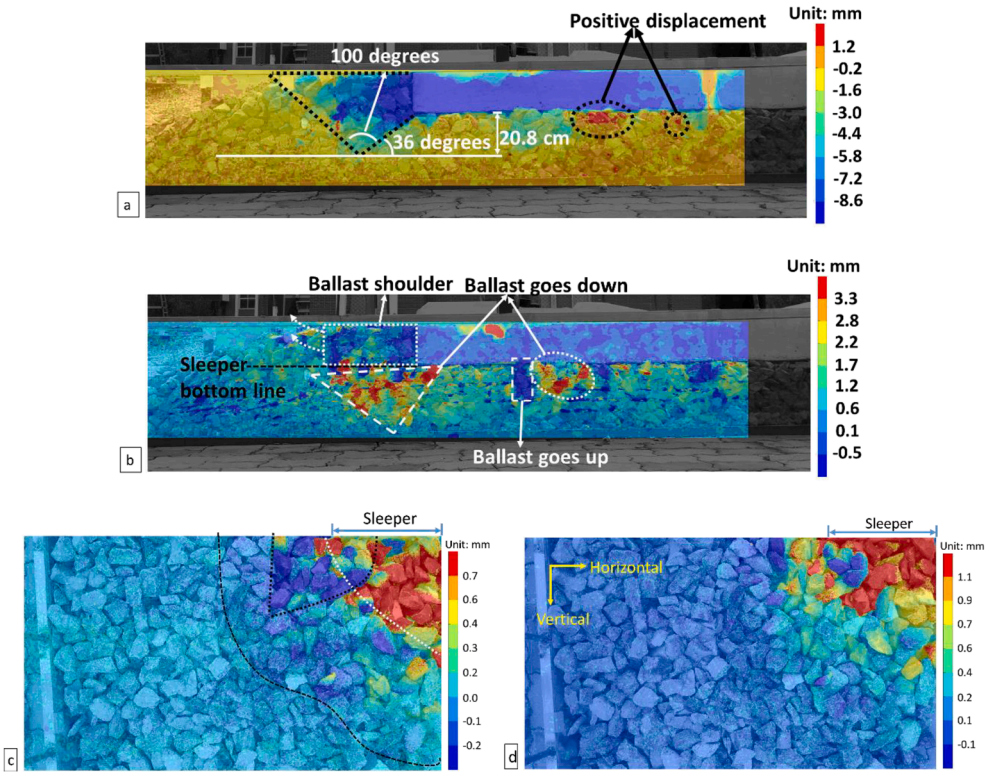

Fig. 16. PIV data of the lateral resistance test (under 7 mm sleeper displacement): a) Side-view of ballast horizontal displacement, b) Side-view of ballast vertical displacement, b) Top-view of the ballast horizontal displacement, d) Top-view of the ballast vertical displacement [34].

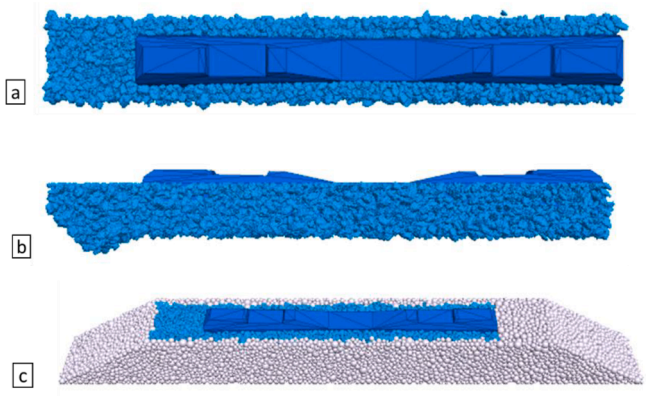

Fig. 17. Optimised multi-layer model of a single sleeper section: a) Top-view of the clump-build layer, b) Side-view of the clump-build layer, c) Over-view of the multi-layer model.

Table 3
Key performance of lateral resistance simulations.

Particle type	Time consuming	Peak lateral force (sleeper)	Maximum contact force (particle)
Clump (Reference model)	43 h 23 min	12.03kN	2.18kN
Multi-layer Half clump/ half ball by height	15 h 45 min	9.92kN	1.56kN
Multi-layer Optimised by most influential ballast area	10 h 25 min	11.20kN	2.93kN
Ball With rolling resistance	2 h 32 min	16.02kN	4.65kN
Ball Without rolling resistance	3 h 05 min	3.76kN	0.37kN

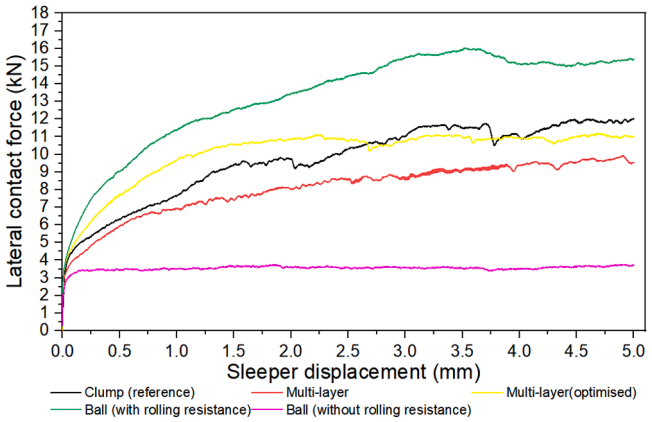

Fig. 18. Sleeper displacement-lateral contact force curve.

range, the force behaviour is proved suitable for ballast simulation.

However, lower stiffness leads to a larger timestep thus less time consuming, so a proper value should be chosen to fit the ballast behaviour of reality. In a low-fidelity model, the irregular shape can be simplified to a ball, and the interlock between particles can be simulated by adding rolling resistance to the linear contact model. The rolling resistance-related parameter is the friction coefficient (or stiffness). With this setting, the rolling effect of a ball can be restricted [25,31,32]. In FPC3D software, the rolling resistance is set by rolling friction. When rolling resistance is added, the contact moment in is Eq. (3) is updated to the Eq. (16). And as shown in Fig. 9.

$$F^l = -F_n^l \hat{n_c} + F_s^l,\ M_c = M^r$$
$$M^r = M^r - k_r \Delta\theta_b \tag{16}$$

Where, M^r is the rolling resistance moment to restrict the rotation,

k_r is the rolling resistance,

$\Delta\theta_b$ is the relative bend-rotation increment of a contact.

In reference [32], the influence of stiffness and rolling friction is analysed by a series of direct shear simulations (ball-built model), and results are shown in the following Fig. 10. In addition, a case of rolling resistance also can be seen in the next chapter, the comparison between 0.3 rolling friction coefficient and without it.

Based on those results, the contact parameters in this paper are listed in the following Table 2.

Efficiency optimisation

With the above-mentioned knowledge, a multi-layer model can be used to improve DEM efficiency. As a case to show the efficiency, the single sleeper section of a ballast track is built.

Firstly, the reference model, using the clump for all particles, is shown in Fig. 11. In this section, the shoulder width is 500 mm, the ballast height (under sleeper) is 350 mm, the shoulder slope is 1:1.75, the top width is 600 mm, and the sleeper is 2600 mm*280 mm*185 mm (L*W*H). This was the commonly used model before optimised. The linear contact model is used, and the contact parameters are listed in Table.2. This model contains 647,323 elements of particles, 86 elements as the sleeper and boundary wall (The boundary wall is shown with the transparency setting and is not displayed in the following models). Related research using this model by the author can be seen in reference [18,33–35]. Thus, its reliability and accuracy have been validated.

Also, a model with ball particles is built, as the additional reference, to show the behaviour loss of shape simplification, as shown in Fig. 12. For this model, with and without rolling resistance are calculated separately. All the contact parameters are shown in Table 2. This model contains 24,394 elements of particles, 86 elements as the sleeper and boundary wall.

Further, the model is simplified by the multi-layer method to reduce the number of elements while keeping relatively high-fidelity results. This method uses the ball shape as ballast in the bottom layer and the irregular shape (clump) in the area where sleeper contact with the ballast. In detail, the lower layer of the ball is 265 mm in height, and the clump layer is 80 mm under the sleeper bottom and 185 mm in the crib. The 80 mm equals 2 times bigger than the average ballast size. It makes sure the sleeper is well-contact with the clump particles.

This method can largely decrease the element number and present the high-fidelity contact between sleeper-ballast. However, the bottom layer is simplified, but rolling resistance is added to the ball-ball contact to simulate the interlock within the irregular particles. The clump-clump contacts model is the linear contact model. All the contact parameters are listed in Table 2. As shown in Fig. 13, this model contains 14,887 elements of balls and 229,222 elements of the clump, which are 264,109 elements of particles in total. The number of elements for the sleeper and boundary wall is 86, which is the same as the reference model. Compared with the model built with clump, this multi-layer model reduces the number of elements by 59%.

Further, the simplification can be optimised depending on the different test types, according to the loading condition (loading controlled test) or displacement condition (displacement controlled test). For example, in a settlement test, the loading condition is vertically applied to the sleeper, and the most influential ballast is located at the bottom of the sleeper. Thus, the bottom ballast particles should be the clump, and other particles (crib and shoulder ballast) can be simplified to the ball. This means the multi-layer model is optimised based on the force distribution. The method is shown in the following Fig. 14.

In order to verify the efficiency and reliability of the optimisation method, the lateral resistance test is simulated with the reference model, the multi-layer model, and the optimised multi-layer. The loading resistance test is displacement controlled. A certain velocity is applied to the sleeper, the direction is lateral and horizontal, and the test is quasi-static status. The target results are the force distribution, lateral resistance, and source contribution (sleeper bottom, end, and side).

In the author's previous work, Particle Image Velocimetry (PIV) was used to analyse the displacement distribution [34]. By this method, the ballast displacement can be obtained through video analysis. As shown in the following Fig. 15, a box of ballast in the dimension of a single sleeper section was used. One side of the box is made of glass. Thus the camera can capture the displacement of ballast particles under the sleeper. Another camera was placed above the ballast shoulder to record that part.

The ballast displacement map is shown in Fig. 16. This result provides the most influenced (displacement) ballast area, which can be used as a guide to building a DEM model. Normally the lateral resistance tests are controlled to stop at 4–5 mm sleeper displacement to better show the ballast behaviour, reference [34] pushed the sleeper to 20 mm. Considering the normal condition, ballast displacement under 7 mm sleeper displacement is enough to be used as guidance in multi-layer modelling.

As shown in Fig. 17, an optimised multi-layer DEM model was built, where the ballast in the most influential area is generated by the clump elements with linear contact model, and other particles are the ball elements with rolling resistance linear contact model. This model-building method makes sure that the number of elements is decreased to the largest extent. It contains 19,358 elements of balls and 131,388 elements of clumps, which are 150,746 elements for particle generation. And the number of elements for the sleeper and the boundary wall is 86. Compared with the reference model (fully clump-built model, in Fig. 10), the total number of elements decreases by 77%.

In order to validate the optimised model, a single sleeper pushing test is conducted on the 3 different models. A lateral velocity is applied to the sleeper, which is 4e-3 mm/s. This low speed ensures the simulation is in a quasi-static state. The weight of the sleeper is 380 kg in the test. In the simulation, the weight is presented by adding a vertical servo force on

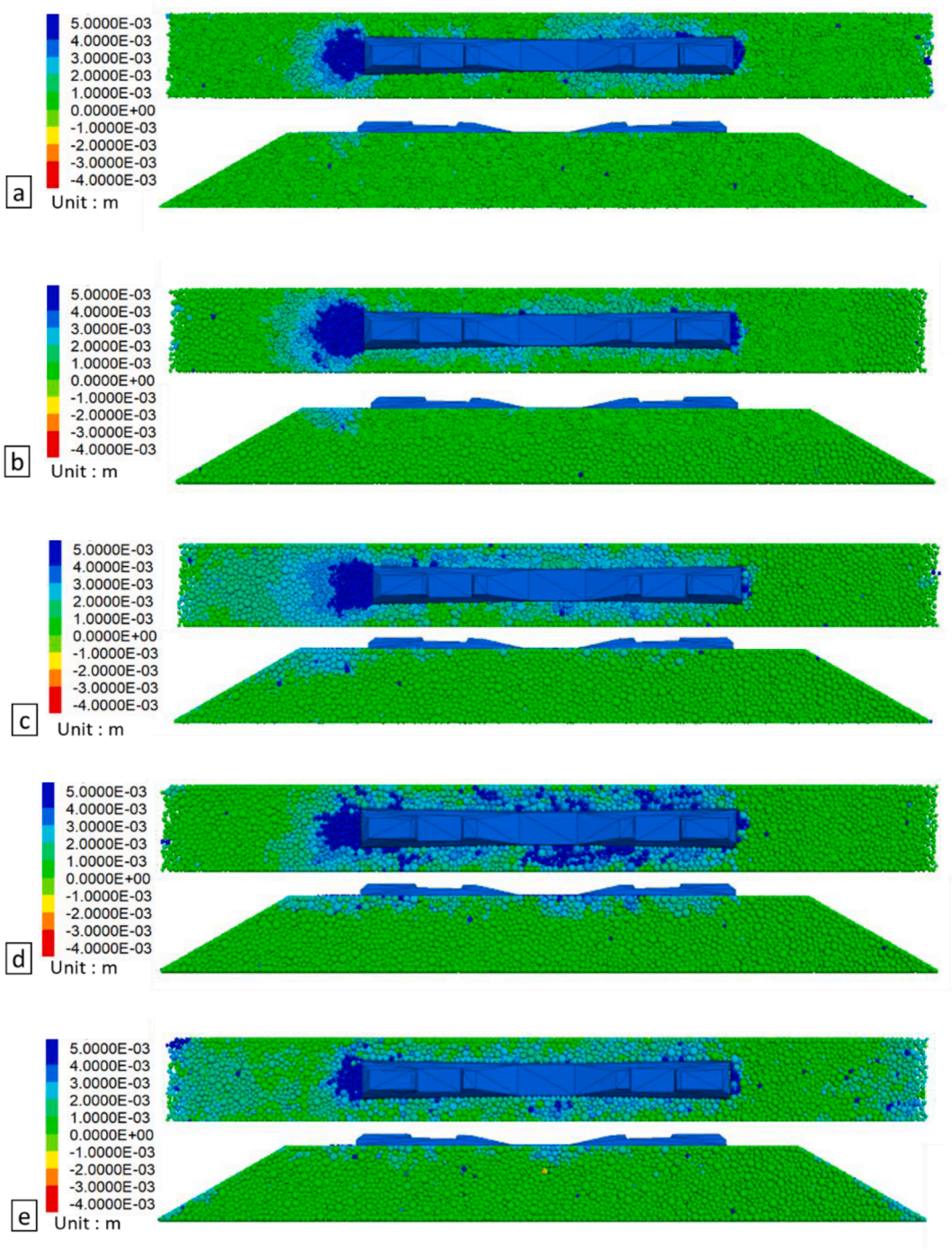

Fig. 19. Ballast displacement after 5 mm sleeper displacement: a) Reference model (all particles are clump), b) Multi-layer model(Half clump and half ball, by height), c) Optimised multi-layer model (based on most influential ballast area), d) Ball-built model (with rolling resistance), e) Ball-built model (without rolling resistance).

the sleeper. The simulation is stopped when the sleeper displacement reaches 5 mm. During this process, the contact force–displacement data of the sleeper is recorded. In addition, the force distribution at the end state is saved to show the difference between each model, thus providing validation. The time consumption shows efficiency. All the simulations were conducted on a workstation with Dual Xeon E5 processor and 64G memory. Results are listed in following Table 3.

In Table 3, the clump-built model costs 43.38 h, whereas the ball model only costs 2.5 and 3 h. This result shows the heavy influence of element number on efficiency. With the optimisation, the efficiency is largely increased. The multi-layer model (half clump and half ball) costs 15.75 h. For the multi-layer model with further optimisation, the time consumption is 10.41 h, and the force behaviour is also the closest to the results of the clump-built model. The force–displacement curves of the sleeper are shown in the following Fig. 18. The increasing trend and peak force between the reference model and the optimised multi-layer model are in a similar state.

On the contrary, the results of the ball-built models (with and without rolling resistance) are all less reliable. The particle displacement at the end of the simulation is shown in Fig. 19, where the ball model with rolling resistance has an extra disturbance on the crib side, which is against the results of the reference model. The force distribution

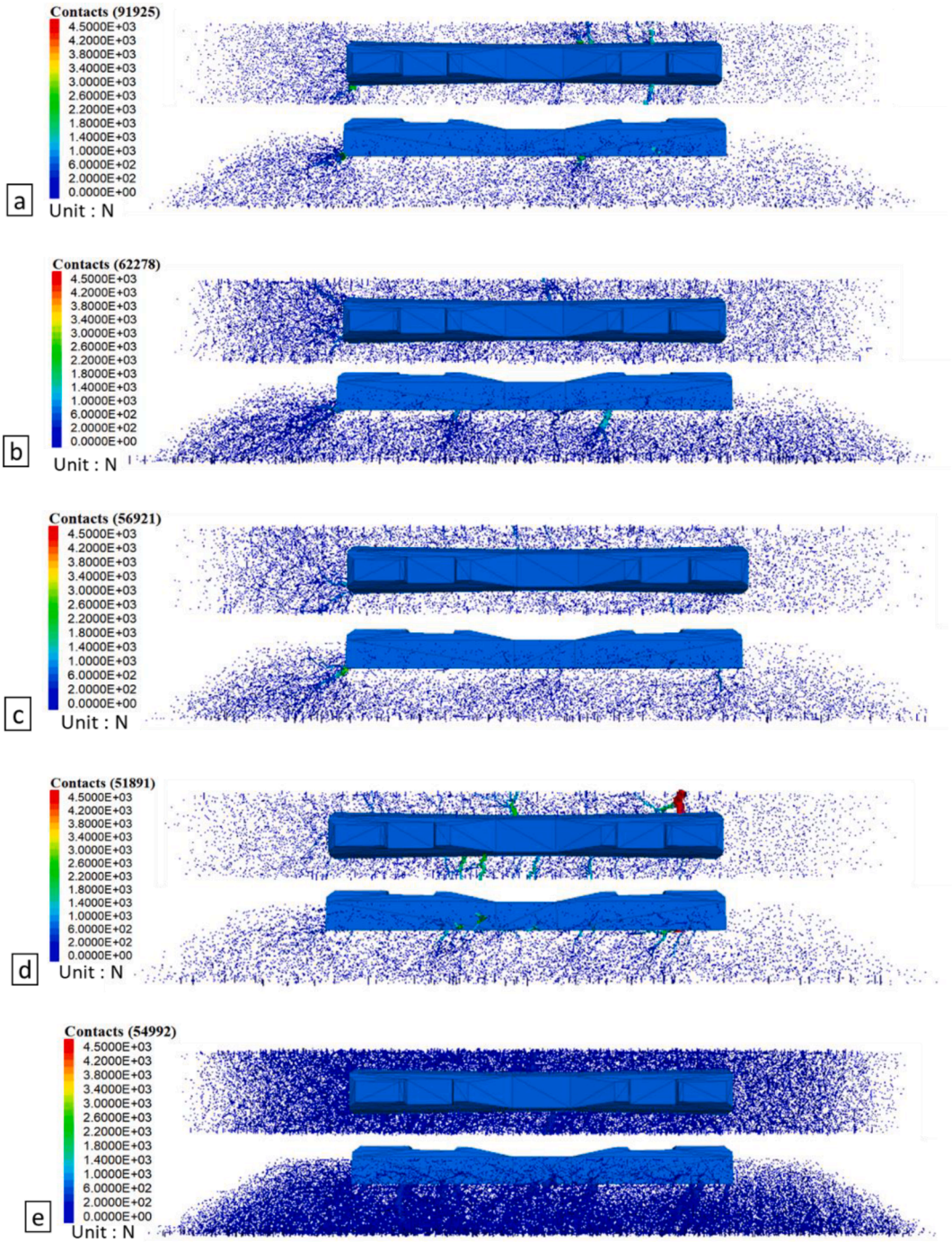

Fig. 20. Contact force chain after 5 mm sleeper displacement: a) Reference model (all particles are clump), b) Multi-layer model(Half clump and half ball, by height), c) Optimised multi-layer model (based on most influential ballast area), d) Ball-built model (with rolling resistance), e) Ball-built model (without rolling resistance).

(Fig. 20) also proves the impossibility of acquiring high reliability using a ball-built model because it shows clear force chains in the crib area but unclear force chains in the shoulder area.

In addition, it can be observed that the added rolling resistance highly increases the peak lateral force from 3.76kN to 16.02kN because the rolling resistance restricts the particle, thus compensating the interlock of angular loss, as expected. The peak lateral force of the ball-built model with the rolling resistance is even higher than the clump-built model. But, it does not mean using a lower value of rolling resistance can reach better fitness. Because the mesoscopic results should also be taken into consideration.

Fig. 19 and Fig. 20 proved the accuracy of the results. The particle displacement is presented. The optimised multi-layer model is very high compared with the results of the reference model. In comparison, other models are not in accordance with the tests. That means the optimised multi-layer model has not only higher efficiency but also higher reliability.

Conclusion

For ballast research, the DEM simulations can provide mesoscopic results. However, the efficiency problem restricts the feasibility of this method. In order to improve the calculation efficiency of DEM, several methods can be used, but all those methods are not proper for ballast

research. With this consideration, this paper explained the importance and influence of particle shape and contact properties of the DEM model for ballast and introduced an optimised multi-layer model-building method. This method, based on the aiming simulations, simplifies the irregular ballast shape to ball shape and uses irregular shape (clump) in the most influential area. As an illustration, to show the accuracy and efficiency of the optimised model, later resistance simulations are used. The results of different models are validated by comparing them with a reference model (clump-build), which is used in the author's previous work. The main conclusions are listed below:

(1) Particle shape in a DEM model influences the force behaviour of the ballast layer. In a ball-build model, the simple particle shape leads to fewer contact numbers and lower contact force. For the clump-built model, the spherical surface of a clump leads to a higher contact number and clear force distribution.
(2) Contact model is the law for force–displacement calculation. Among those parameters, stiffness influences calculation efficiency, and the rolling resistance (rolling friction) applied to a ball element can restrict the rolling behaviour, thus maintaining the loss of irregular shape.
(3) However, the rolling resistance can compensate for the interlock loss of irregular shape, but the reliability of force distribution and particle displacement is low.
(4) The idea of the optimised multi-model is to decrease the number of elements used in a model. It is realised by using irregular shapes in the most influential area and balls in other areas. The case shows this method can increase efficiency and keep accuracy.
(5) The most influential area is different for different simulations. Therefore, selecting the proper area is the first step of model building. The selection should be based on the type of simulations and the target results. In this paper, the lateral resistance is simulated, and the most influential area is defined by particle displacement, which is obtained by previous tests using the PIV method.

CRediT authorship contribution statement

Wenli Jia: . **Valeri Markine:** Supervision, Methodology. **Yunlong Guo:** Supervision.

Declaration of Competing Interest

The authors declare that they have no known competing financial interests or personal relationships that could have appeared to influence the work reported in this paper.

Data availability

Data will be made available on request.

Acknowledgement

This is from work undertaken as part of the IN2ZONE project, which has received funding from the Shift2Rail Joint Undertaking (JU) under grant agreement 101014571 – IP/ITD/CCA – IP3.

References

[1] Esveld C. Modern railway track. The Netherlands: MRT-Productions; 2001.
[2] Indraratna B. Advanced Rail Geotechnology-Ballasted Track. CRC Press; 2011.
[3] Wang H, Markine V. Modelling of the long-term behaviour of transition zones: Prediction of track settlement. Eng Struct 2018;156:294–304.
[4] Wang H, Markine V, Liu X. Experimental analysis of railway track settlement in transition zones. Proc Inst Mech Eng F J Rail Rapid Transit 2018;232(6):1774–89.
[5] Huang H, Brennecke B. Track Stiffness Transition Zone Studied with Three-Dimensional Sandwich Track Model. Transport Res Rec: J Transport Res Board 2013;2374(1):136–42.
[6] Indraratna B, Ionescu D, Christie HD. Shear behaviour of railway ballast based on large Scale triaxial tests. J Geotech Geoenviron Eng 1998;124(5):439–49.
[7] Lu M, McDowell GR. The importance of modelling ballast particle shape in the discrete element method. Granul Matter 2006;9(1–2):69–80.
[8] Jing GQ, Aela P, Fu H, Yin H. Numerical and experimental analysis of single tie push tests on different shapes of concrete sleepers in ballasted tracks. Proc Inst Mech Eng, Part F: J Rail Rapid Transit 2018;233(7):666–77.
[9] V. Toropov, V. Markine, The use of simplified numerical models as mid-range approximations, 6th Symposium on Multidisciplinary Analysis and Optimization, 1996.
[10] Lucia DJ, Beran PS, Silva WA. Reduced-order modeling: new approaches for computational physics. Prog Aerosp Sci 2004;40(1–2):51–117.
[11] Jin R, Du X, Chen W. The use of metamodeling techniques for optimization under uncertainty. Struct Multidiscip Optim 2003;25(2):99–116.
[12] Lommen S, Mohajeri M, Lodewijks G, Schott D. DEM particle upscaling for large-scale bulk handling equipment and material interaction. Powder Technol 2019;352:273–82.
[13] Mak J, Chen Y, Sadek MA. Determining parameters of a discrete element model for soil–tool interaction. Soil Tillage Res 2012;118:117–22.
[14] Wang X, Zhang S, Pan H, Zheng Z, Huang Y, Zhu R. Effect of soil particle size on soil-subsoiler interactions using the discrete element method simulations. Biosyst Eng 2019;182:138–50.
[15] Gong H, Song W, Huang B, Shu X, Han B, Wu H, et al. Direct shear properties of railway ballast mixed with tire derived aggregates: Experimental and numerical investigations. Constr Build Mater 2019;200:465–73.
[16] Huang H, Tutumluer E, Dombrow W. Laboratory Characterization of Fouled Railroad Ballast Behavior. Transport Res Rec: J Transport Res Board 2009;2117(1):93–101.
[17] Indraratna B, Ngo NT, Rujikiatkamjorn C, Vinod JS. Behavior of Fresh and Fouled Railway Ballast Subjected to Direct Shear Testing: Discrete Element Simulation. Int J Geomech 2014;14(1):34–44.
[18] Jia W, Markine V, Guo Y, Jing G. Experimental and numerical investigations on the shear behaviour of recycled railway ballast. Constr Build Mater 2019;217:310–20.
[19] Wang J, Gutierrez M. Discrete element simulations of direct shear specimen scale effects. Géotechnique 2010;60(5):395–409.
[20] Mahmoud E, Papagiannakis AT, Renteria D. Discrete Element Analysis of Railway Ballast under Cycling Loading. Procedia Eng 2016;143:1068–76.
[21] Guo Y, Ji Y, Zhou Q, Markine V, Jing G. Discrete Element Modelling of Rubber-Protected Ballast Performance Subjected to Direct Shear Test and Cyclic Loading. Sustainability 2020;12(7):2836.
[22] Chen C, McDowell GR. An investigation of the dynamic behaviour of track transition zones using discrete element modelling. Proc Inst Mech Eng, Part F: J Rail Rapid Transit 2014;230(1):117–28.
[23] Hossain Z, Indraratna B, Darve F, Thakur PK. DEM analysis of angular ballast breakage under cyclic loading. Geomech Geoeng 2007;2(3):175–81.
[24] Coetzee C. Calibration of the discrete element method: Strategies for spherical and non-spherical particles. Powder Technol 2020;364:851–78.
[25] Aela P, Zong L, Esmaeili M, Siahkouhi M, Jing G. Angle of repose in the numerical modeling of ballast particles focusing on particle-dependent specifications: Parametric study. Particuology 2022;65:39–50.
[26] Chen J, Gao R, Liu Y. Numerical Study of Particle Morphology Effect on the Angle of Repose for Coarse Assemblies Using DEM. Adv Mater Sci Eng 2019;2019:1–15.
[27] Obermayr M, Vrettos C, Eberhard P, Däuwel T. A discrete element model and its experimental validation for the prediction of draft forces in cohesive soil. J Terramech 2014;53:93–104.
[28] Bian X, Li W, Qian Y, Tutumluer E. Micromechanical Particle Interactions in Railway Ballast through DEM Simulations of Direct Shear Tests. Int J Geomech 2019;19(5):04019031.
[29] Khatibi F, Esmaeili M, Mohammadzadeh S. DEM analysis of railway track lateral resistance. Soils Found 2017;57(4):587–602.
[30] Guo Y, Zhao C, Markine V, Jing G, Zhai W. Calibration for discrete element modelling of railway ballast: A review. Transp Geotech 2020;23:100341.
[31] Ai J, Chen J-F, Rotter JM, Ooi JY. Assessment of rolling resistance models in discrete element simulations. Powder Technol 2011;206(3):269–82.
[32] Guo Y, Zhao C, Markine V, Shi C, Jing G, Zhai W. Discrete element modelling of railway ballast performance considering particle shape and rolling resistance. Railw Eng Sci 2020;28(4):382–407.
[33] Jing G, Zhang X, Jia W. Lateral resistance of polyurethane-reinforced ballast with the application of new bonding schemes: Laboratory tests and discrete element simulations. Constr Build Mater 2019;221:627–36.
[34] Guo Y, Jia W, Markine V, Jing G. Rheology study of ballast-sleeper interaction with particle image Velocimetry (PIV) and discrete element modelling (DEM). Constr Build Mater 2021;282:122710.
[35] Jing G, Jia W, Wang X, Markine V, Nålsund R, Guo Y. Experimental and numerical study on lateral resistance of frictional sleeper with arrowhead groove. Transp Geotech 2021;30:100638.